九州大学学術情報リポジトリ
Kyushu University Institutional Repository

Impact of Stepped Hull Design on Speed Boat Performance: A CFD Study

Yeddid Yonatan Eka Darma
Department of Ship Manufacturing Engineering, Politeknik Negeri Banyuwangi

Raditya Hendra Pratama
Research Center for Energy Conversion and Conservation, National Research and Innovation Agency

I.G.N.A Satria Prasetya Dharma Yudha
Department of Ship Manufacturing Engineering, Politeknik Negeri Banyuwangi

Andhi Indira Kusuma
Department of Naval Architecture, Institut Teknologi Adhi Tama Surabaya

https://doi.org/10.5109/7236898

出版情報：Evergreen. 11 (3), pp.2580-2589, 2024-09. 九州大学グリーンテクノロジー研究教育センター
バージョン：
権利関係：Creative Commons Attribution 4.0 International

Impact of Stepped Hull Design on Speed Boat Performance: A CFD Study

Yeddid Yonatan Eka Darma[1,*], Raditya Hendra Pratama[2], I.G.N.A Satria Prasetya Dharma Yudha[1], Andhi Indira Kusuma[3]

[1]Department of Ship Manufacturing Engineering, Politeknik Negeri Banyuwangi, Indonesia

[2]Research Center for Energy Conversion and Conservation, National Research and Innovation Agency, Indonesia

[3]Department of Naval Architecture, Institut Teknologi Adhi Tama Surabaya, Indonesia

*Author to whom correspondence should be addressed:
E-mail: yeddidyonatan@poliwangi.ac.id

(Received May 12, 2024: Revised July 2, 2024: Accepted August 2, 2024).

Abstract: As the demand for tourism boat services on the Karang-Sewu Bali to Marina Boom Banyuwangi route surges due to the increasing number of tourists from Bali wishing to explore Eastern Java's Banyuwangi, the need for a faster and more efficient mode of transportation with a strong emphasis on safety becomes imperative. This study focuses on the analysis of speed boat design, specifically examining the impact of stepped hull design on performance. We investigate the lift generated by the boat at various speeds and assess how the hull's lift affects the total drag of the vessel, all in pursuit of the optimal design within the proposed framework. Our objective is to determine the boat design that offers the highest efficiency and the shortest travel time to the destination. Leveraging the Numeca CFD software, we analyze lift generation, compare results, and provide a detailed explanation of the optimal design. This research seeks to enhance the tourism boat experience on this route, ultimately benefiting both passengers and service providers.

Keywords: Optimum Boat Design; Hull Performance; Stepped Hull; CFD Analysis; Sustainable Maritime Transportation

1. Introduction

Efficient and swift transportation systems are vital for optimizing tourism experiences, especially in regions with high travel demand[1,2]). The Marina Boom Banyuwangi - Karang Sewu Bali route stands out as a prominent tourist destination, highlighting the need for a customized tourist boat to facilitate travel and minimize potential delays during peak holiday periods. From the standpoint of a travel agency, the best way to maximize fuel oil consumption during periods of high travel should be considered.

Meanwhile, as the government focuses on reducing carbon emissions, the type of boat hull plays a crucial role in supporting this effort by influencing optimal ship speed and fuel oil consumption efficiency[3–7]). In academia and industry, there has been a recent surge in interest in boat hull performance as it relates to boat resistance and propulsion. The need to optimize fuel efficiency is the main factor that drives speed boat design optimization, which has favorable effects on both cost savings and environmental preservation.

Planing hulls are widely chosen for their high-speed performance, maneuverability, and stability, making them ideal for water activities that prioritize speed and agility[8–12]). Because of these properties, planing hulls are popular for a variety of recreational and sporting activities. There are several methods for calculating the hydrodynamic characteristics of planing hulls, including experimental, analytical, and computational methods.

Many theoretical investigations and experimental hydrodynamic characteristics of planing hulls have been conducted currently, for instance, the research from Begovic and Bertorello[13]), which discussed the experimental study of prismatic and warped planing hulls without verification and validation with simulation analysis. They indicated a range of speeds at which the hydrodynamic resistance is not considerably impacted by the warping of the hull bottom or the higher deadrise angles of the hull's forward section. On the other side, Matveev[14]) analyzed the analytical study of negative and positive deadrise warped planing hulls. The analytical results demonstrated that, when the side wetted-surface of such a hull is removed, its lift and drag characteristics are quite comparable to those of a hull with the same negative and positive deadrise.

In 2017, De Marco et al.[15]) discussed experimental and numerical analysis of a stepped planing hull and the

related fluid dynamics phenomena typically occurring in the stepped hull in the unwetted aft body area behind the step. Their research indicated that a unique vortex pattern existed in the dry rear section for a scaled single-step hull model during towing tank experiments. Concurrently, comparable flow patterns were identified in numerical simulations with a detailed 3D flow analysis on a fine mesh study. Niazmand Biandi et al.[16] also investigated the experimental and numerical analysis of the hydrodynamic forces of single-stepped planing hulls. They emphasized that the numerical analysis employing 2D + T theory has an acceptable accuracy in motion prediction of single-stepped planing hulls, which can assist engineers in the early stages of a stepped planing hull design process. Computational techniques are generally less expensive than experimental tests and more dependable than analytical/empirical methods. As a result, Computational Fluid Dynamics (CFD) tools are now frequently utilized and regarded as effective, particularly during the early stages of design[17–19].

Recent advancements in Al-6063 surface composites (ASCs) through Friction Stir Processing (FSP) have shown significant improvements in hardness and tensile strength, crucial for automotive as well as marine applications. The incorporation of graphene nano-powder and multi-pass FSP techniques have resulted in homogenous dispersion of particulates, reduced grain size, and enhanced mechanical properties [20]. Parallel to these material advancements, intelligent and sustainable manufacturing practices are revolutionizing production. Technologies such as digital twins, predictive maintenance, AI-driven intelligent factories, and green manufacturing methods are enhancing efficiency and reducing environmental impact. These innovations optimize design, quality control, and supply chain sustainability, integrating advanced simulations and real-time data analytics [21]. Together, these advancements in material science and manufacturing technologies hold significant potential for optimizing speed boat hull designs through comprehensive CFD analysis of lift and drag parameters, promoting more efficient and sustainable maritime engineering solutions.

This research aims to investigate the consequences of incorporating a stepped hull (planing hull type) modification (involving three variations of the hull model) on the performance of a tourist boat, with a specific emphasis on lift generation and its impact on total drag. The overarching objective is to design a 5 Gross Tonnage (GT) tourist ship that ensures enhanced efficiency, resulting in quicker travel times and a more enriched experience for tourists exploring the captivating waters between Banyuwangi and Karang-Sewu Bali. To validate the design modifications, CFD software will be employed to scrutinize lift generation and its relationship with hull drag across different speeds. Through a comparative analysis of these results, we aim to pinpoint the optimal hull configuration for the 5 GT tourist ships. The insights obtained from this study are expected to provide valuable perspectives for the development of high-speed passenger boat models within the tourism sector by analyzing the vessel's performance based on lift and drag parameters, with regard to the wetted surface area. Consequently, this study can offer a cost-effective alternative for evaluating vessel performance.

2. Methodology

2.1.Main Approach to Ship Design

There are two basic methods in ship design for initial estimation, namely the relational or empirical method, and the parametric method[22,23]. Determination of the main dimensions with the empirical method is based on comparative data from ships that have been built previously, with data from sources or public information (web search), commercial and internal databases, and available ship data files. A variation of this method is the use of empirical design formulas deduced through the adjustment of relevant statistical regression diagrams or properly defined design coefficients, with the help of previously searched vessel data[24].

To shape the ship's hull, both below the waterline and superstructure, a series of design parameters are needed, which are numerically identifiable measurements and become boundary values. It should be noted that the formation of the shape of the hull includes several parameter values that become a reference. Several ship design parameters are set and defined in Eq.1 as follows[25]:

$$Cb = 0.70 + \frac{1}{8}\left(\tan^{-1}\frac{(23-100Fn)}{4} radians\right) \quad (1)$$

where Cb is the ship's block coefficient, and Fn is the Froude number.

Ship resistance is characterized as the opposing force encountered by a ship in motion, arising from the friction between the hull and the surrounding fluid[26–29]. Among the prominent factors contributing to resistance in ships, viscous resistance stands out prominently, primarily induced by the impact of fluid viscosity. Within viscous resistance, two principal elements come into play: frictional resistance and resistance originating from the shape of the ship's hull[30]. The total resistance R_T is expressed in Eq.2 as follows:

$$R_T = C_T \times 0.5 \times \rho \times {v_s}^2 \times S \quad (2)$$

where C_T is the total coefficient of resistance, ρ is sea water density, vs is the ship's service speed, and S is wetted surface area.

Drag force is a force that inhibits the movement of a solid object[31], where the drag force is a component of the resultant force or a force that acts parallel to the direction of fluid movement but is inversely proportional to the

cross-sectional area of the object and the velocity of the fluid flow. The drag force F_D itself is defined by the following formula in Eq.3[11]:

$$F_D = C_D \times 0.5 \times \rho \times {v_s}^2 \times S \quad (3)$$

where C_D is the ship's drag coefficient.

Lift is the resultant force that is perpendicular to the direction of the fluid flow velocity[32,33]. An object immersed in a fluid flow will experience forces due to the interaction of the fluid with the object; the force generated is in the form of a normal force caused by changes in pressure and shear forces that occur due to fluid viscosity. When viewed from the horizontal direction, the force perpendicular to the direction of flow is called lift. The lift force can be expressed by the formula in Eq.4[34]:

$$F_L = C_L \times 0.5 \times \rho \times {v_s}^2 \times S \quad (4)$$

where C_L is the ship's lift coefficient.

2.2.Computational Fluid Dynamics (CFD) Simulation

Computational Fluid Dynamics (CFD) is one of the calculation methods in the control of dimensions, area, and volume by utilizing computer assistance in performing calculations on each of the dividing elements. The CFD structure consists of 4 software modules that require geometries and meshes to provide the information needed to perform CFD analysis. The use of CFD for experimental purposes provides more advantages when compared to experiments using models. Time efficiency and an unlimited number of tests and the results can be obtained with accuracy. CFD components include a preprocessor as part of the physics preprocessor, followed by a solver that is linked to the solver manager as part of solving or running simulations, and a post-processor which is a module to display simulation results coupled with various flow visualizations[35].

The flow solver, in this CFD simulation is based on the fundamental Navier-Stokes equations, which govern the behavior of fluid flow by describing the relationships between pressure, velocity, and density. These equations can be numerically solved to simulate various fluid dynamics phenomena. For incompressible flows, the Navier-Stokes equations and the continuity equation, which ensures time continuity, can be mathematically represented as follows:

$$\frac{\partial u_i}{\partial x_i} = 0 \quad (5)$$

Where u_i is the time-averaged velocity components in Cartesian directions, and x_i is the Cartesian coordinates.

$$\frac{\partial u_i}{\partial t} + \frac{\partial (u_i u_j + u"_i u"_j)}{\partial x_i} = R_i - \frac{1}{\rho}\frac{\partial p}{\partial x_i} + \frac{\partial}{\partial x_j}\left(v\left(\frac{\partial u_i}{\partial x_j} + \frac{\partial u_j}{\partial x_i}\right)\right) \quad (6)$$

$$v = \frac{\mu}{\rho} \quad (7)$$

where t is time, R_i is the volume force, p is the time average pressure, v is kinematic viscosity, μ is dynamic viscosity, ρ is the density of water.

Solving the mass conservation equation and Newton's second law, also known as the momentum conservation equation, gives us the velocity and pressure fields. The continuous formulation for mass conservation may be invalid on a discrete grid, and an alternative derivation using the discrete divergence is proposed. Additionally, the study of turbulent flows reveals the existence of small-scale routes for the flow of energy, indicating the presence of both forward and inverse energy cascades, which are crucial in understanding the momentum conservation dynamics.

For the mass conservation:

$$\frac{d}{dt}\iiint_D \rho dv = 0 \quad (8)$$

where D is the fluid domain, dv is an arbitrary control volume

For the momentum conservation:

$$\frac{d}{dt}\iiint_D \rho \vec{U} dv = \iiint_D \rho \overrightarrow{f_v} dv + \iint_D \vec{T} dS \quad (9)$$

where $\overrightarrow{f_v}$ is volume force (normally gravity force), S is the strain rate, and $\vec{T}$ is a constraint, i.e., $\vec{T} = \sigma \times \vec{n}$, where σ is the constraint tensor and $\vec{n}$ is the unit normal vector [36].

In CFD, the mesh serves as a numerical grid that discretizes the computational domain into small geometric elements (Fig. 1). The size of these elements, known as the mesh size, plays a pivotal role in CFD simulations. When visualizing the mesh structure in a pre-processor, the varying sizes are especially noticeable near objects within the domain. This intentional refinement of mesh near solid surfaces is crucial for accurately capturing the boundary layer, a thin region adjacent to the surface where fluid properties experience rapid changes. The mesh size is not uniform throughout the domain; it is typically finer near objects and coarser in less critical areas. This graded approach helps in capturing intricate flow patterns, turbulence, and fluid-solid interactions. In summary, the non-uniform mesh sizing, especially near objects, is a deliberate strategy to enhance the accuracy of CFD simulations, particularly in regions where fluid dynamics exhibit significant variations. In the subsequent post-processing phase, a thorough analysis of the fluid flow is performed. The residuals of the numerical solution are plotted over the simulation time to ensure the solution's convergence.

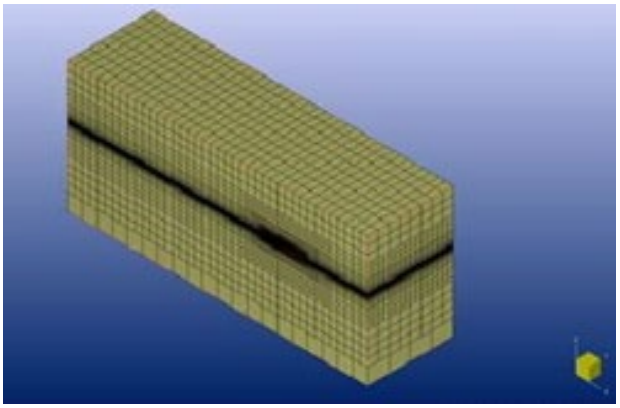

Fig. 1: Pre-Processor CFD

In this CFD simulation, testing will be carried out on each hull model to determine the effect of variations in the hull on the lift and drag forces. The simulation stage begins with making a model of the hull with the help of 3D Modeling software and then exporting it to a step file with the extension .stp, then the next stage is making boundary layers, and setting other parameters. For this simulation, the ship speed is assumed at several speed variations, namely 12 knots, 16 knots, and a maximum speed of 20 knots.

Basically, on CFD-based software, the analysis stage itself is generally divided into 4 stages, namely geometry settings, pre-processor, solver manager, and post-processor. For the boundary layer, this simulation refers to the International Towing Tank Conference reference, the size of the boundary layer can be seen in Fig. 2.

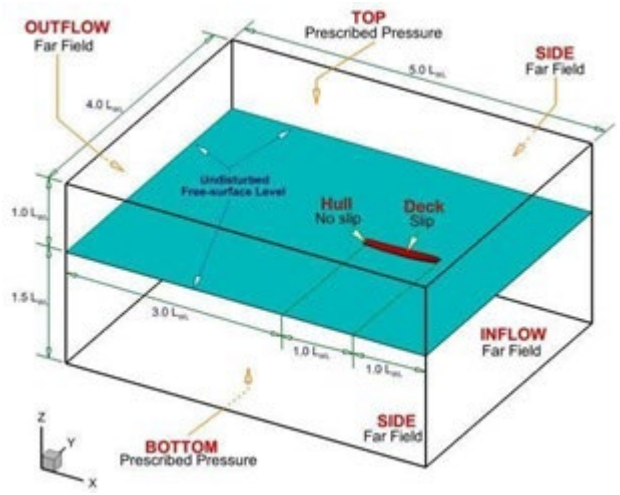

Fig. 2: Boundary Layer

2.3.Determination of the Main Size of the Ship

In this research, the principal size is determined based on statistical methods using linear regression (empirical method). Based on the data obtained from several comparison ships, the ship size, speed, and passenger capacity are obtained. The regression process is started by making a graph from the comparison ship data where the abscissa (x) is the passenger capacity and the ordinate (y) is the main size of the ship so that later it becomes a comparison graph between capacities vs ship length, capacity vs ship width, and so on[37].

In the initial and final phases of ship design, the accurate estimation of diverse weight categories and the determination of the ship's centroids are pivotal considerations. Potential inaccuracies or oversights in these computations may exert a significant impact on the vessel's cargo transport capacity, speed, stability, and overall safety throughout its maritime journey. Rigorous scrutiny of weight distribution and centroid positioning is imperative to ensure precise calculations align with engineering standards, thereby contributing to the optimization of vessel performance and adherence to safety protocols in the transportation of goods at sea[24].

In determining the main size of this ship, the author took a sample of 10 comparison ships. It can be seen in the comparison ship table in Table 1. Furthermore, the comparison ship data is regressed linearly to obtain an approach to the main size of the ship which will later be used as a reference in determining the size of the ship to be designed. The ship dimensions are shown in Table 2

Table 1. Ships Reference.

Ship Name	Length (m)	Breadth (m)	Height (m)	Draught (m)
Laboan Bajo	10.0	2.5	1.20	0.40
Blue Ocean 001	12.0	2.7	1.40	0.45
Bintang Laut	9.0	2.2	1.00	0.35
Marine 1030	10.0	2.6	1.20	0.40
Bintuni Pemda	9.0	2.2	1.10	0.35
Marine 1025	10.0	2.5	1.20	0.45
Sea Pearl	10.5	2.6	1.25	0.45
JS 7022	10.0	2.5	1.50	0.45
Raden Segoro	10.0	2.5	1.20	0.45
Ouner PS boat	10.5	2.6	1.20	0.40

Table 2. Ships Dimension from Regression Result.

Main Dimension	Regression Result	Determined Dimension	Unit
Length	10.20	10.20	m
Breadth	2.50	2.50	m
Height	1.31	1.30	m
Draught	0.50	0.50	m

2.4.3D Hull Model

The 3D model is made after the main size of the ship has met the ratio value. Making a 3D model is required to have a coefficient value that is close to or equal to the coefficient value in the previous calculation. Therefore, the main dimensions of the ship have been determined to investigate the interest of the study, as shown in Table 3.

Table 3. Main Dimensions of the Ship.

Information	Value	Unit
Length Overall (LOA)	10.20	m
Length Between Perpendicular (LPP)	8.73	m
Length of Waterline (LWL)	8.66	m
Breadth (B)	2.50	m
Height (H)	1.30	m
Draught (T)	0.50	m
Block Coefficient (C_b)	0.508	-
Midship Coefficient (C_m)	0.613	-
Prismatic Coefficient (C_p)	0.829	-
Displacement	5.56	Ton
Volume	5.28	m^3
Service Speed (v_s)	20	Knot

Abbas Dashtimanesh's investigation[38], underscores the persisting challenges in achieving precise simulations of various fluid flow phenomena inherent to the two-step hull. Notably, accurate representations of ventilation, flow separation from steps, multiphase flow, and water spray behind the steps demand more nuanced consideration. Extending upon this research, our paper offers a distinctive perspective, assessing the appropriateness of one-stepped hulls versus two-stepped hulls for the tourism sector. Within our study, we present and analyze three distinct hull options.

The representation of the ship model, incorporating a stepped hull in three dimensions, is conducted in two stages. The initial phase involves creating a hull model using a 3D modeler, with three variations designated for lift force and drag force analysis in this study. In hull variation A, the reference is the original design, a standard hull without any stepped hull modifications. Hull variation B constitutes a modification of the initial design, featuring a stepped hull applied to the 8th frame of the ship, with a stepped hull height of 0.1 meters and an increase in the baseline behind the stepped hull of 0.05 meters. As for hull variation C, the modification involves applying a stepped hull at the 6th frame of the ship, with a stepped hull height of 0.1 meters. Figure 3 illustrates the 3D design images for each hull variation resulting from these modifications.

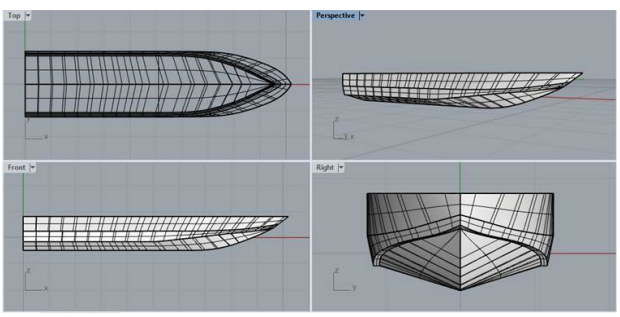

(a) Hull Variation A

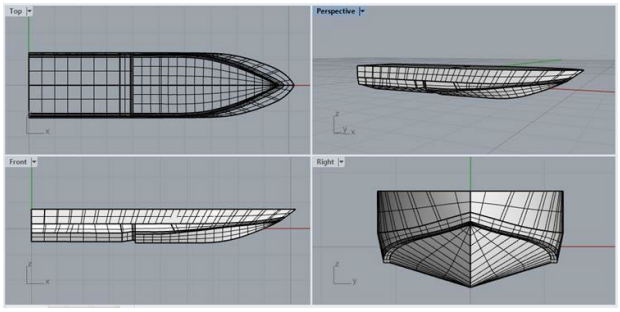

(b) Hull Variation B

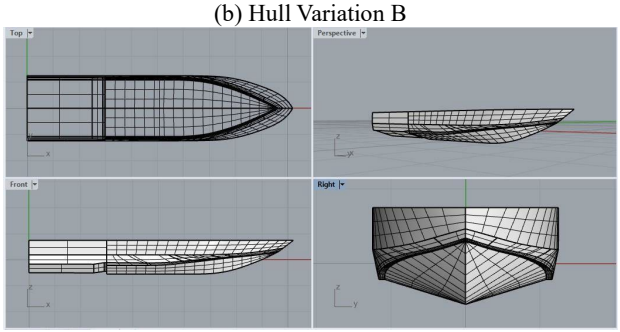

(c) Hull Variation C

Fig. 3: Hull Design Variations Included Stepped Hull

3. Result and Discussion

In numerical simulations, validating the results is crucial. One key indicator of the validity of a numerical simulation is the residual result. Residuals represent the difference between the left and right sides of the discretized equations, effectively measuring the error at each iteration step. To ensure the accuracy of our simulation, we conducted a convergence assessment by monitoring the decrease in residuals, as illustrated in Fig. 4. A significant and steady decrease in residuals with increasing iterations generally indicates that the solution is converging. In our study, the residual values for one of the conditions decreased substantially and reached a steady state after approximately 4500 iterations out of the 5000 iterations conducted. This behavior suggests that the numerical solution is approaching the true solution of the discretized equations, thus validating the reliability of our simulation results.

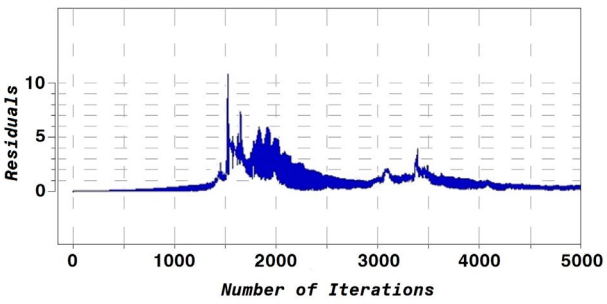

Fig. 4: Convergence Assessment on the Numerical Simulation

The CFD simulation provides insights into the drag force and lift force for various hulls at different service

speeds, illustrated in Fig. 5 (a) and (b), respectively. Analyzing the graphs reveals a notable trend: an increase in ship service speed correlates with an exponential rise in drag force, as indicated by Equation (4). However, this deviates from the expectations for a quadratic equation due to the concurrent decrease in the wetted surface area.

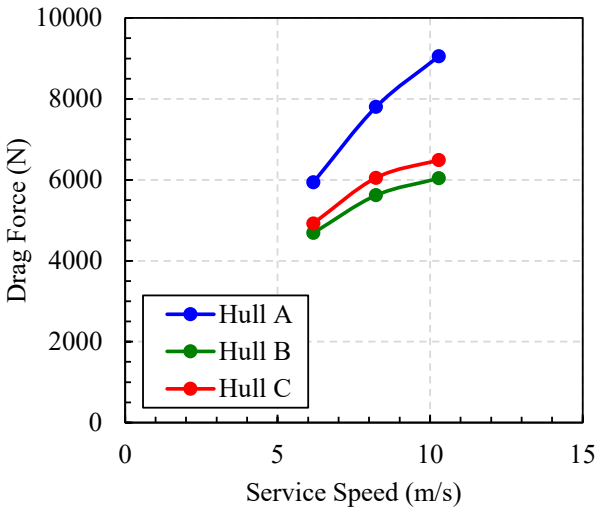

(a) Drag Force

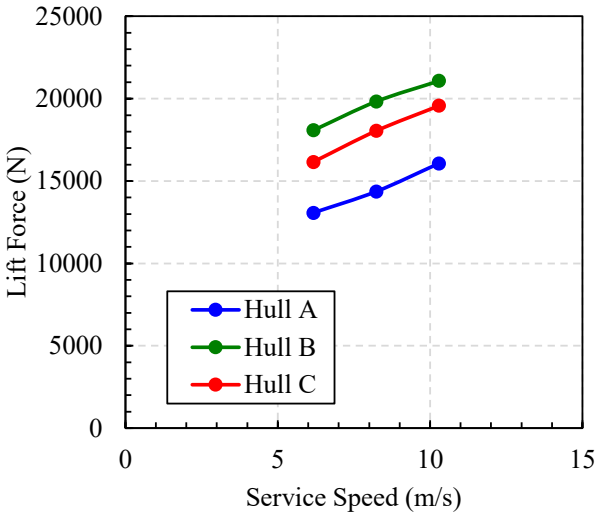

(b) Lift Force

Fig. 5: Drag Force and Lift Force across Different Hulls and Service Speeds

Among the three hull variations examined, Hull Variation A, without the addition of a stepped hull, exhibits the highest drag force. In contrast, Hull Variation B, featuring a stepped hull on the 8th frame, experiences the lowest drag force. Notably, Hull Variation C, with a stepped hull on the 6th frame, records a slightly larger drag force compared to Hull Variation B.

Figure 5 (b) illustrates the lift force results for each hull variation at various service speeds. Similar to drag force trends, lift force increases with the rise in service speed. Despite this increase not following an exponential pattern due to the diminishing wetted surface area, an interesting observation emerges in terms of hull variations. Hull Variation B produces the highest lift force, followed by Hull Variation C and then Hull Variation A. This suggests that the application of a stepped hull enhances lift force, contributing to a reduction in drag force.

Figure 6 illustrates the wetted surface results for various service speeds and hull variations. The analysis of the wetted surface area aims to discern its impact on the drag force and lift force values corresponding to each hull variation. The graph reveals that an increase in service speed correlates with a decrease in wetted surface area. Comparatively, the ship without a stepped hull exhibits the largest wetted surface area. Consequently, it can be deduced that the wetted surface area is consistently inversely proportional to lift force due to the lifted hull, resulting in the subsequent reduction of the submerged hull area.

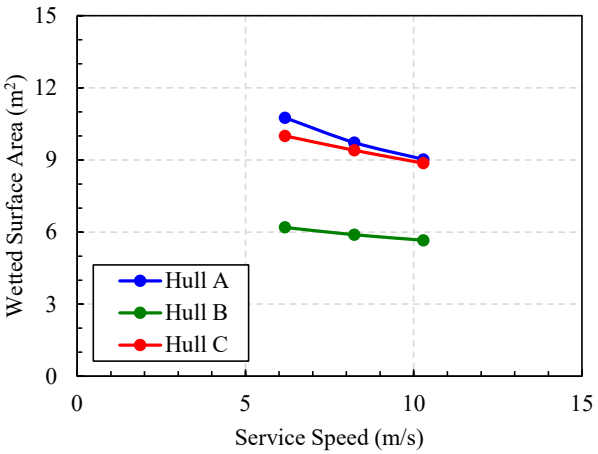

Fig. 6: Wetted Surface Area across Different Hulls and Service Speeds

Through CFD simulation, the hull area is subjected to fluid flow, with colors in the visualization indicating the magnitude of the mass fraction of water on the hull. The redder the color, the greater the water mass fraction in that section, highlighting the strong interaction between the hull and fluid flow. Figure 7 presents a comparative analysis of water mass fraction and wet surface area across all hulls at specified speed variations. The images reveal that, with increasing ship speed, mass fraction decreases in the fore hull area, resulting in pressure concentration toward the stern. The red portion accumulating at the stern indicates a lifted bow position, with the center of pressure shifting to the stern hull. As discussed earlier, this coincides with the observed decrease in wet hull area as ship speed increases.

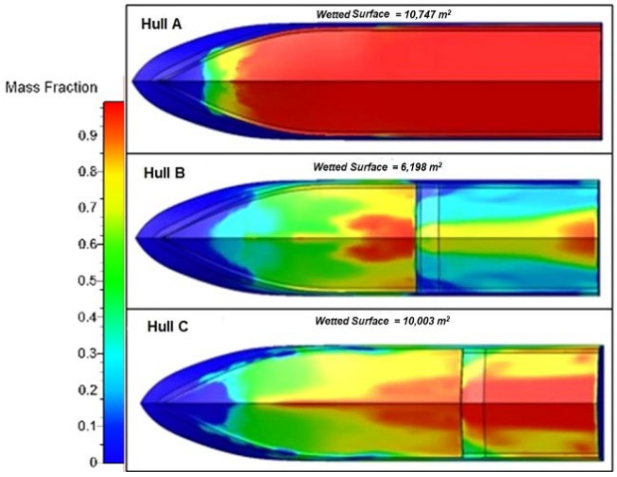

(a) v_s = 6.2 m/s (12 knot)

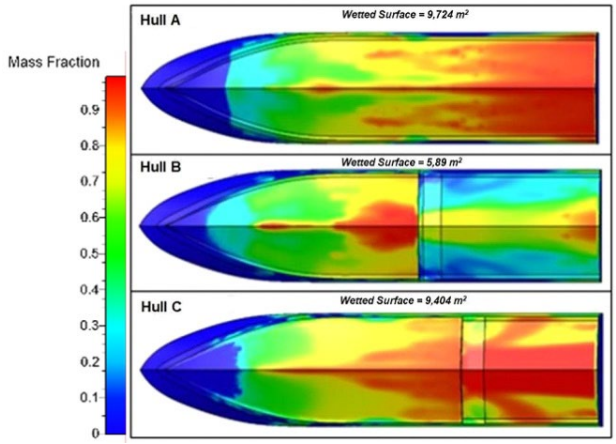

(b) v_s = 8.2 m/s (16 knot)

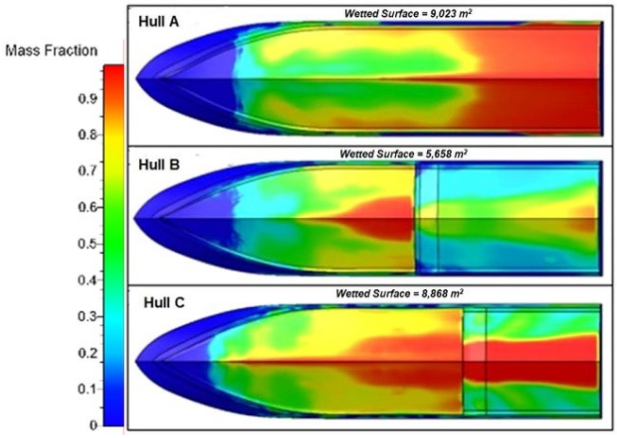

(c) v_s = 10.3 m/s (20 knot)

Fig. 7: Water Mass Fraction and Wetted Surface Area for Various Hulls and Service Speeds

The application of a stepped hull on the ship has been validated by CFD results, demonstrating a reduced wet surface area compared to the ship without a stepped hull. It is both interesting and crucial to investigate the percentage decrease in wetted surface area across hull variations. The calculation involved determining the average hull area across all speeds and assessing the percentage of decline, as presented in Table 4. Additionally, Table 5 provides a comprehensive summary of CFD simulation results, including wetted surface area, drag force, drag coefficient, lift force, and lift coefficient.

Table 4. Reduction Percentage of Wetted Surface Area.

Speed (m/s)	Reduction from Hull A to Hull B	Reduction from Hull A to Hull C
6.2	42.4%	7.0%
8.2	39.4%	3.3%
10.3	37.3%	1.7%
Average	39.7%	4.0 %

As depicted in Table 4, Hull B exhibits a significant 39.7% mean decrease in wet hull area compared to Hull A, while Hull C experiences a more modest 4.0% decrease. However, an examination of Hull B's water mass fraction area, as illustrated in Fig. 6, reveals friction, particularly in the middle and stern regions. This suggests that the ship may encounter jerks, impacting passenger comfort at high speeds due to partial hull detachment from the water. Drawing on the previous research[39–41], optimal fluid flow at high speeds involves nearly complete wetting of the hull bottom and surrounding areas, minimizing air interaction for stable ship movement.

In consideration of these factors, Hull B, despite its low drag force and high lift force compared to Hull A and Hull C, was not chosen for the future research design since the design will be applied to a tourism boat. Figure 6 indicates that friction in Hull C is more evenly distributed in the stern and surrounding areas, suggesting that this hull variation allows for stable movement at high speeds. Consequently, this study adopts Hull C for future research with a drag coefficient of 13.5 and a lift coefficient of 40.7, as outlined in Table 5.

Table 5. Summary of CFD Simulation Result.

Speed (m/s)	Wetted Surface Area (m^2)					
	Hull A	Hull B	Hull C			
6.2	10.8	6.2	10.0			
8.2	9.7	5.9	9.4			
10.3	9.0	5.7	8.7			
Speed (m/s)	**Drag-Force (N)**			**Drag Coefficient**		
	Hull A	Hull B	Hull C	Hull A	Hull B	Hull C
6.2	5938	4688	4923	0.028	0.038	0.025
8.2	7806	5620	6052	0.023	0.027	0.018
10.3	9059	6039	6493	0.018	0.018	0.013
Speed (m/s)	**Lift Force (N)**			**Lift Coefficient**		
	Hull A	Hull B	Hull C	Hull A	Hull B	Hull C
6.2	13069	18062	16154	0.062	0.149	0.082
8.2	14359	19830	18043	0.042	0.097	0.055
10.3	16064	21082	19570	0.032	0.068	0.040

While wetted surface area is a crucial factor influencing the drag coefficient, our study recognizes the significant

impact of the stepped hull design, particularly on Hull B. The stepped hull contributes to a high wake formation behind it, resulting in an elevated drag coefficient.

Figure 8 shows the wave elevation generated by the boat with different hull types at a vessel speed of 20 knots (10.3 m/s). As seen in the figures for Hull B and Hull C, there are localized increases in wave elevation due to the sudden change in hull geometry, resulting in a series of peaks and troughs in the wave pattern. The wave elevation generated by the stepped hull results in more complex wave interactions and energy dissipation compared to a hull without steps. As the vessel moves through the water, the divergent and transverse waves generated by the hull interfere with each other, leading to constructive and destructive interference effects. Constructive interference, where wave crests align, creates larger waves that require more energy to overcome, thus increasing residual resistance. Additionally, the energy expended in creating these waves directly contributes to the overall energy loss, highlighting the substantial role that wave patterns play in the total resistance experienced by the vessel.

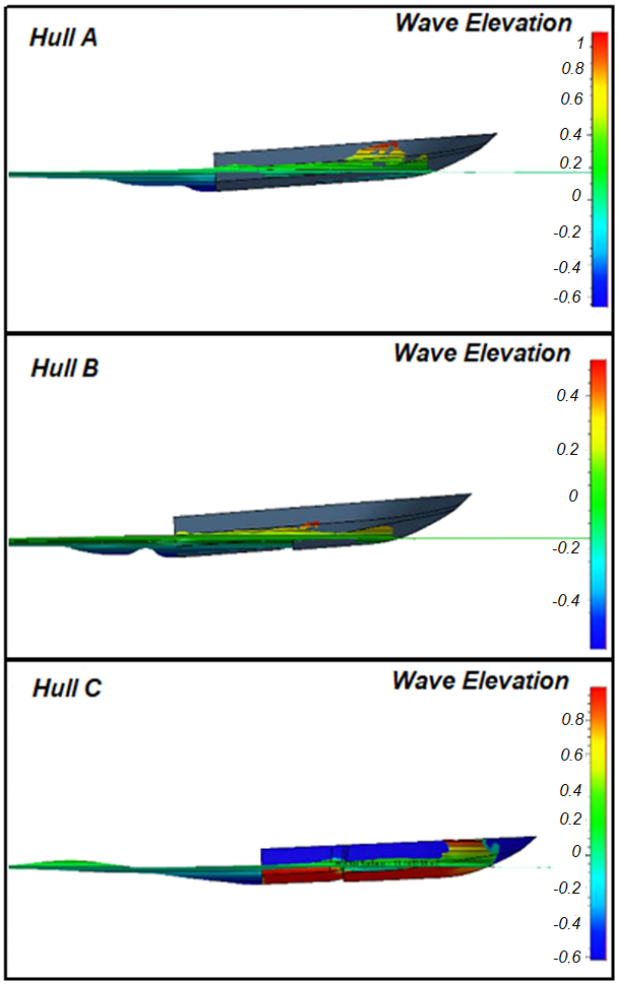

Fig. 8: Wave Elevation Generated by the Boat at Different Hull Types at a Vessel Speed of 20 Knots (10.3 m/s)

We acknowledge that the simulation results currently lack a detailed explanation of why the placement of the stepped hull influences the outcomes. To address this, we plan to conduct an additional analysis on the streamline, specifically investigating the variations in results when altering the location of the stepped hull.

4. Conclusions

Upon completion of the design and analysis procedures outlined in this paper, the authors draw conclusive insights regarding the investigated tourist ship's design. The outcomes of the Computational Fluid Dynamics (CFD) simulations on three different hull variations reveal a consistent inverse relationship between lift and drag forces. The higher lift generated by the hull corresponds to lower drag force, indicating that substantial lift results in relatively diminished total ship resistance.

The application of the stepped hull across the three hull variations, analyzed for lift force and drag force, highlights that Hull B, featuring a stepped hull on frame 8, exhibits lower drag force and higher lift force compared to Hulls A and C. Hull B demonstrates a 41.17% reduction in wet hull surface area compared to Hull A and a 6.26% decrease compared to Hull C. However, it is noted that Hull B, despite its favorable characteristics, shows signs of reduced friction in the middle and stern areas, potentially leading to discomfort for passengers at high speeds due to hull detachment from water.

In light of these findings, the study concludes that Hull C is the most viable option for the tourist ship's design. Hull C demonstrates a more evenly distributed friction profile around the stern, indicating stable movement at high speeds. The design will be further examined by an experimental test as the next step of this research. In conclusion, this research by CFD simulation marks a significant stride toward advancing the understanding of ship performance, with a particular focus on the dynamic jumping conditions experienced at high speeds.

Acknowledgments

The authors express their gratitude for the facilities, scientific, and technical support provided by Politeknik Negeri Banyuwangi Ship Design Laboratory. Special thanks are extended to Mr. Nova Husnanda for generously providing the Ship Hull Design utilized in this study.

Nomenclature

C_b	Ship block coefficient (–)
F_n	Froude number (–)
R_T	Ship total resistance (kN)
C_T	Total coefficient of resistance (–)
ρ	Sea water density (kg/m^3)
V_s	Service speed (Knot)
S	Wetted surface area (m^3)
C_D	Ship's drag coefficient (–)

C_L Ship's lift coefficient (–)

References

1) J.-W. Yu, Y.-G. Lee, A.-S. Park, Y. jin Ha, C. Park, and Y.-C. Choi, "A study on the resistance performance of korean high-speed small coastal fishing boat," *Journal of The Society of Naval Architects of Korea*, **48** 158–164 (2011). https://api.semanticscholar.org/CorpusID:56420161.
2) M.T. FARRIS, and D.O.N. WELCH, "High-speed ship technology: maritime vessels for the 21st century," *Transportation Journal*, **38** (*1*) 5–14 (1998). http://www.jstor.org/stable/20713369.
3) A.S. Husain, "Improving Hull Design for Better Efficiency and Environmental Protection," in: 2014. https://api.semanticscholar.org/CorpusID:199604235.
4) A. Nugroho, B. Al Hakim, D. Priatno, C. Sasmito, T. Muttaqie, A. Tjolleng, I. Iskendar, M. Kurniawan, and S. Komariyah, "Mission analysis of small-scale lng carrier as feeder for east indonesia: ambon city as the hub terminal," *Evergreen*, **10** 1938–1950 (2023). doi:10.5109/7151748.
5) H. Zakerdoost, and H. Ghassemi, "A multi-level optimization technique based on fuel consumption and energy index in early-stage ship design," *Structural and Multidisciplinary Optimization*, **59** (*5*) 1417–1438 (2019). doi:10.1007/s00158-018-2136-7.
6) M.A. Lutfi, A.R. Prabowo, E.M. Muslimy, T. Muttaqie, N. Muhayat, H. Diatmaja, Q.T. Do, S.J. Baek, and A. Bahatmaka, "Leisure boat concept design: study on the influence of hull form and dimension to increase hydrodynamic performance," *International Journal of Mechanical Engineering and Robotics Research*, **13** (*1*) 139–161 (2024). doi:10.18178/ijmerr.13.1.139-161.
7) F. Tillig, J.W. Ringsberg, W. Mao, and B. Ramne, "Analysis of uncertainties in the prediction of ships' fuel consumption – from early design to operation conditions," *Ships and Offshore Structures*, **13** (*sup1*) 13–24 (2018). doi:10.1080/17445302.2018.1425519.
8) S. Tavakoli, M. Zhang, A.A. Kondratenko, and S. Hirdaris, "A review on the hydrodynamics of planing hulls," *Ocean Engineering*, **303** 117046 (2024). doi:https://doi.org/10.1016/j.oceaneng.2024.117046.
9) A.Z. Ashkezari, and M. Moradi, "Three-dimensional simulation and evaluation of the hydrodynamic effects of stern wedges on the performance and stability of high-speed planing monohull craft," *Applied Ocean Research*, **110** 102585 (2021). doi:https://doi.org/10.1016/j.apor.2021.102585.
10) S.M. Sajedi, and P. Ghadimi, "Experimental investigation of the effect of two steps on the performance and longitudinal stability of a mono-hull high-speed craft," *Cogent Eng*, **7** (*1*) (2020). doi:10.1080/23311916.2020.1790980.
11) S.M. Mousaviraad, Z. Wang, and F. Stern, "URANS studies of hydrodynamic performance and slamming loads on high-speed planing hulls in calm water and waves for deep and shallow conditions," *Applied Ocean Research*, **51** 222–240 (2015). doi:https://doi.org/10.1016/j.apor.2015.04.007.
12) J.-Y. Park, H. Choi, J. Lee, H. Choi, J. Woo, S. Kim, D.J. Kim, S.Y. Kim, and N. Kim, "An experimental study on vertical motion control of a high-speed planing vessel using a controllable interceptor in waves," *Ocean Engineering*, **173** 841–850 (2019). doi:https://doi.org/10.1016/j.oceaneng.2019.01.019.
13) E. Begovic, and C. Bertorello, "Resistance assessment of warped hullform," *Ocean Engineering*, **56** 28–42 (2012). doi:https://doi.org/10.1016/j.oceaneng.2012.08.004.
14) K.I. Matveev, "Hydrodynamic modeling of planing hulls with twist and negative deadrise," *Ocean Engineering*, **82** 14–19 (2014). doi:https://doi.org/10.1016/j.oceaneng.2014.02.021.
15) A. De Marco, S. Mancini, S. Miranda, R. Scognamiglio, and L. Vitiello, "Experimental and numerical hydrodynamic analysis of a stepped planing hull," *Applied Ocean Research*, **64** 135–154 (2017). doi:10.1016/j.apor.2017.02.004.
16) R.N. Bilandi, S. Mancini, L. Vitiello, S. Miranda, and M. De Carlini, "A validation of symmetric 2d + t model based on single-stepped planing hull towing tank tests," *J Mar Sci Eng*, **6** (*4*) (2018). doi:10.3390/jmse6040136.
17) S. Mancini, A. Dashtimanesh, R. Niazmand Bilandi, F. Di Caterino, and M. Carlini, "A Numerical Way for a Stepped Planing Hull Design and Optimization," in: Proceedings of NAV 2018: 19th International Conference on Ship and Maritime Research, 2018. doi:10.3233/978-1-61499-870-9-220.
18) T. Fu, K. Brucker, M. Mousaviraad, C. Ikeda-Gilbert, E.J. Lee, T.T. O'Shea, Z. Wang, F. Stern, and C. Judge, "An Assessment of Computational Fluid Dynamics Predictions of the Hydrodynamics of High-Speed Planing Craft in Calm Water and Waves," in: 30th Symposium on Naval Hydrodynamics, 2014.
19) M. Kandasa, S.K. Ooi, P. Carrica, F. Stern, E. Campana, D. Peri, P. Osborne, J. Cote, N. Macdonald, and N. de Waal, "CFD validation studies for a high-speed foil-assisted semi-planing catamaran," *J Mar Sci Technol*, **16** 157–167 (2011). doi:10.1007/s00773-011-0120-7.
20) P. Kumar, V. Sharma, D. Kumar, and S. Akhai, "Morphology and mechanical behavior of friction stirred aluminum surface composite reinforced with graphene," *Evergreen*, **10** (*1*) 105–110 (2023). doi:10.5109/6781056.
21) S. Akhai, "Navigating the potential applications and challenges of intelligent and sustainable manufacturing for a greener future," *Evergreen*, **10** (*4*) 2237–2243 (2023). doi:10.5109/7160899.
22) S. Han, Y.S. Lee, and Y.B. Choi, "Hydrodynamic hull

form optimization using parametric models," *J Mar Sci Technol*, **17** (*1*) 1–17 (2012). doi:10.1007/s00773-011-0148-8.
23) A. Papanikolaou, "Ship Design - Methodologies of Preliminary Design," SPRINGER, 2014. doi:10.1007/978-94-017-8751-2.
24) D. Majnarić, S. Baressi Šegota, N. Anđelić, and J. Andrić, "Improvement of machine learning-based modelling of container ship's main particulars with synthetic data," *J Mar Sci Eng*, **12** (*2*) (2024). doi:10.3390/jmse12020273.
25) D.G.M. Watson, "Practical Ship Design," Elsevier, 1998.
26) A. Lindholdt, K. Dam-Johansen, S.M. Olsen, D.M. Yebra, and S. Kiil, "Effects of biofouling development on drag forces of hull coatings for ocean-going ships: a review," *J Coat Technol Res*, 415–444 (2015). doi:10.1007/s11998-014-9651-2.
27) R. Cooke, "An experimental investigation into the components of ship resistance," University of Cape Town, 1986.
28) M.F. Syahrudin, M.A. Budiyanto, and M.A. Murdianto, "Analysis of the use of stern foil on the high speed patrol boat on full draft condition," *Evergreen*, **7** (*2*) 262–267 (2020). doi:10.5109/4055230.
29) A.F. Molland, S.R. Turnock, and D.A. Hudson, "Ship Resistance and Propulsion: Practical Estimation of Propulsive Power," Cambridge University Press, Cambridge, 2011. doi:DOI: 10.1017/CBO9780511974113.
30) Edward V. Lewis, "Principles of Naval Architecture," SNAME, 1988.
31) H. Anam, L. Haris, A. Budiyarto, and A. Budiyono, "Design of diver propulsion vehicle ganendra ri-1 using solidworks flow simulation," *Marine and Underwater Science and Technology*, **1** 55–60 (2015).
32) Y. Cui, J. Ravnik, O. Verhnjak, M. Hriberšek, and P. Steinmann, "A novel model for the lift force acting on a prolate spheroidal particle in arbitrary non-uniform flow. part ii. lift force taking into account the non-streamwise flow shear," *International Journal of Multiphase Flow*, **111** 232–240 (2019). doi:https://doi.org/10.1016/j.ijmultiphaseflow.2018.12.003.
33) N.I. Ismail, M.A. Tasin, H. Sharudin, M.H. Basri, S.C. Mat, H. Yusoff, and R.E.M. Nasir, "Computational aerodynamic investigations on wash out twist morphing mav wings," *Evergreen*, **9** (*4*) 1090–11021 (2022). doi:10.5109/6625721.
34) C. YANG, F. HUANG, and F. NOBLESSE, "Practical evaluation of the drag of a ship for design and optimization," *J Hydrodynam B*, **25** (*5*) 645–654 (2013). doi:https://doi.org/10.1016/S1001-6058(13)60409-6.
35) J. Blazek, "Computational Fluid Dynamics: Principles and Applications," Elsevier Science, 2001.
36) A.M. Chiroșcă, and L. Rusu, "Comparison between model test and three cfd studies for a benchmark container ship," *J Mar Sci Eng*, **9** (*1*) 1–16 (2021). doi:10.3390/jmse9010062.
37) Edward V. Lewis, "Principle of Naval Architecture Second Edition Volume II," Society of Naval Architects and Marine Engineers, 2009.
38) A. Dashtimanesh, A. Esfandiari, and S. Mancini, "Performance prediction of two-stepped planing hulls using morphing mesh approach," *Journal of Ship Production and Design*, **34** 1–13 (2018). doi:10.5957/jspd.160046.
39) F. Cucinotta, D. Mancini, F. Sfravara, and F. Tamburrino, "The effect of longitudinal rails on an air cavity stepped planing hull," *J Mar Sci Eng*, **9** (*5*) (2021). doi:10.3390/jmse9050470.
40) D.J. Clark, W.M. Ellsworth, and J.R. Meyer, "The Quest for Speed at Sea," n.d. https://www.foils.org/wp-content/uploads/2018/01/NSRDC-Quest-for-speed.pdf (accessed May 11, 2024).
41) L. Yun, and A. Bliault, "High Performance Marine Vessels," 1st ed., Springer New York, NY, n.d. doi:https://doi.org/10.1007/978-1-4614-0869-7.